Check for updates

OPTICA

Transient light shift register mechanism of bi-chromatic pulse generation

Boris Nyushkov,[1,2] Aleksey Ivanenko,[1] Sergey Smirnov,[1] and Sergey Turitsyn[3,*]

[1]*Novosibirsk State University, Novosibirsk, 630090, Russia*
[2]*Novosibirsk State Technical University, Novosibirsk, 630073, Russia*
[3]*Aston Institute of Photonic Technologies, Aston University, Birmingham, B4 7ET, UK*
*s.k.turitsyn@aston.ac.uk

Primary methods for generating short pulses in lasers require intracavity elements or physical mechanisms for modulation or the saturable absorption of radiation. This often complicates laser design and limits capabilities, particularly beyond single-wavelength operation. We propose and explore a method for the synchronous generation of bicolor, high-repetition-rate pulses that combines stimulated emission from Yb rare-earth ions and Raman scattering in a shared all-fiber laser cavity, without employing saturable absorbers or modulators. The proposed mechanism for pulsed lasing is analogous to an optical shift register, with two pulse trains shifting relative to each other by one period after every round trip. This naturally solves the critical problem of compensating for the dispersion-induced differential delay of bi-chromatic pulses during an intracavity round trip. The shift register inherently enables stationary generation of bi-chromatic pulses with a common relatively high repetition rate that is inversely proportional to the differential delay. We have demonstrated the feasibility of the proposed technique through the stable generation of sub-nanosecond bi-chromatic (1066 and 1241 nm) pulses with a repetition rate exceeding 166 MHz. The proposed approach is rather general, and we anticipate that it can facilitate more affordable bi-chromatic pulse generation in a variety of laser systems.

1. INTRODUCTION

Short light pulses play a crucial role in various scientific and industrial applications. The mechanisms of pulse formation from noise in lasers, or more broadly, the emergence of patterns, are of interest for both fundamental physics and laser technology. Mode-locking and *Q*-switching are the two primary methods used for generating short pulses in lasers. Pulse generation is enabled through either the active modulation of laser parameters (via an intracavity modulator) or the mechanism of saturable absorption, where intracavity losses are reduced at high optical intensities. Saturable absorption can be implemented using materials with appropriate nonlinear properties, for instance, semiconductors, carbon nanotubes, graphene, MoS_2, WS_2, black phosphorous, MXene, and so on [1], or by exploiting the various physical mechanisms and nonlinear cavity arrangements, such as nonlinear loop mirrors or nonlinear polarization evolution [2]. The incorporation of modulators or saturable absorbers into lasers generally complicates the system design and imposes additional limits on energy and spectral characteristics of lasing. We introduce here, to the best of our knowledge, a new pulse generation mechanism that does not require any saturable absorbers or modulators. Moreover, the established transient light shift register mechanism facilitates stationary pulse generation synchronously at two different wavelengths within a single laser. Our numerical modeling indicates that this proposed method is rather versatile and could be implemented in various all-fiber or hybrid (bulk/fiber) laser systems.

The development of efficient methods for bicolor (dual-wavelength) pulse generation is important for applications such as distance measurements [3], other LIDAR-based measurements [4], coherent pulse synthesis [5], pump–probe experiments [6], coherent anti-Stokes Raman spectroscopy [7], and for accessing the mid- and far-infrared via differential frequency generation or other nonlinear parametric processes [8]. All-fiber bicolor laser solutions are particularly attractive due to their reliability, efficiency, and high-quality output.

There are several basic approaches to bicolor pulse generation in fiber lasers. Dual-wavelength passively mode-locked lasing can be implemented using stimulated emission from a single rare-earth-doped active fiber that provides relatively wideband amplification [9–11]. This family of bicolor lasers features a rather moderate separation (<100 nm) of the lasing wavelengths and typically requires precise adjustment of intracavity transmission characteristics, most often via polarization control, for proper dual-wavelength pulsed operation. These types of light sources do not provide strict synchronization of pulse repetition rates at two different lasing wavelengths.

Another common approach relies on incorporating two different rare-earth-doped active fibers into a joint cavity with a shared saturable absorber. This setup enables stimulated-emission-based pulsed lasing at significantly different wavelengths, for instance, at 1.03 and 1.53 µm [12], or at 1.55 and 1.88 µm [13]. This method typically requires considerably more elaborate experimental efforts compared to the single rare-earth-doped active fiber system. Although this approach allows synchronization of pulse repetition rates, it requires precise adjustment of the relative length of cavity branches with different active fibers [12]. Furthermore, the wavelength availability is still limited to the amplification bands of the rare-earth-doped fibers.

Lasing in spectral intervals beyond the rare-earth bands can be achieved using Raman amplification. Optical fibers doped for a significant extension of the Raman frequency shift, such as P_2O_5-fibers [14,15], are of particular interest in the development of pulsed lasers. Several synchronously pumped Raman laser schemes using P_2O_5-fibers have already been demonstrated [16–18]. The typical technique includes a mode-locked rare-earth-doped fiber laser and an external fiber-resonator-based Raman converter. This configuration demands a precise adjustment of the Raman resonator length to align the group delay of the Stokes pulses with the repetition rate of the pumping laser. Aside from the experimental complexity, this approach has relatively moderate energy efficiency because the chromatic dispersion in the Raman resonator decreases the effective interaction length of pump and Stokes pulses. The pulse repetition rates achievable in this type of bicolor fiber laser source are determined by the pumping lasers and typically do not exceed several dozens of MHz.

There have also been several successful demonstrations of dual-wavelength pulsed lasing by sustaining stimulated emission from rare-earth ions and associated Raman emission in a shared fiber cavity [19–21]. The challenges of implementing these single-cavity bicolor pulsed lasers stem from two critical requirements. The first is the need to design and adjust artificial saturable absorbers for optimal pulse shaping, with a trade-off between pulsed lasing characteristics at the fundamental and Stokes waves. The second requirement is the need to precisely compensate for the differential group delay (DGD) acquired by the fundamental and Stokes pulses after every intracavity round trip. DGD compensation is necessary for the stationary generation relying on repeatable interaction of the same fundamental and Stokes pulses after each round trip. Pulse repetition rates in these single-cavity lasers are also limited to just several MHz by their cavity lengths.

Here, we present and examine a novel method for achieving stationary bi-chromatic high-repetition-rate (>100 MHz) pulsed lasing in a single-cavity fiber laser. The proposed mechanism is analogous to an optical shift register, with two-wavelength pulse trains shifting relative to each other by one pulse period after every round trip. This effectively solves the problem of compensation for DGD of bi-chromatic pulses at the intracavity round trip. We demonstrate that the shift register facilitates synchronous pulsed generation at two significantly different wavelengths with the same repetition rate being inversely proportional to the intracavity DGD.

Shaping of the fundamental and Stokes pulses through this new mechanism is a simultaneous, self-consistent process that occurs entirely in a lengthy Raman fiber. It is initially triggered by the instability of intracavity Raman conversion of continuous-wave (CW) fundamental radiation. As a result, synchronous generation of sub-nanosecond pulses at 1066 and 1241 nm with a common repetition rate (initially at 166.3 MHz and ultimately at 249.1 MHz) was achieved in our test-bed laser configuration, without the use of any saturable absorbers or modulators.
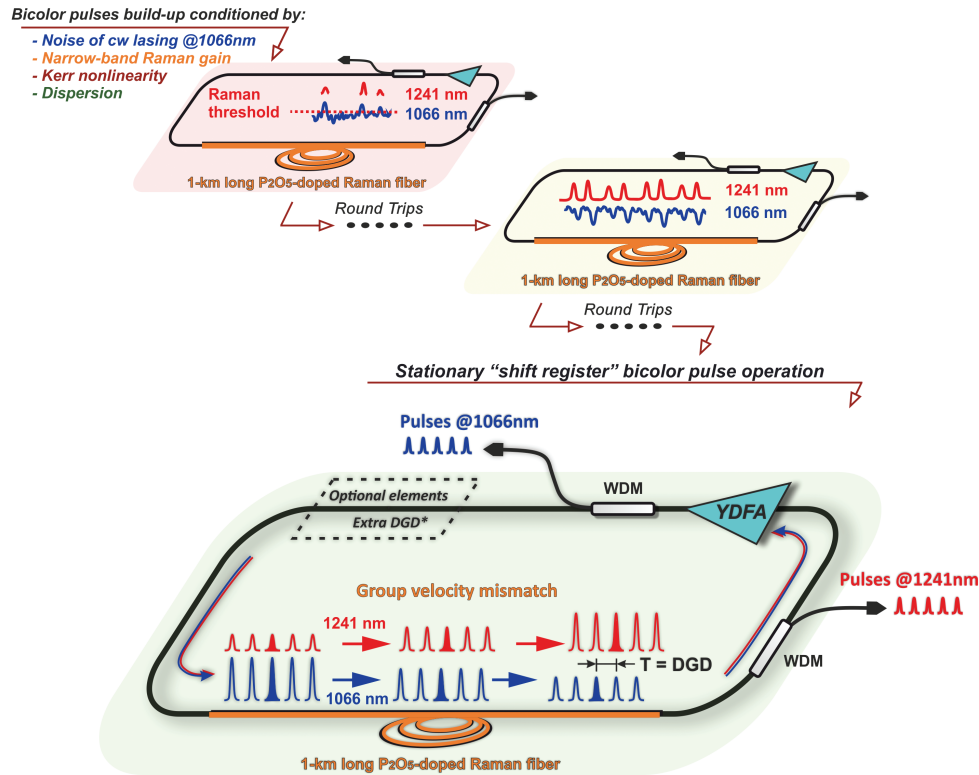
2. PRINCIPLE OF THE SHIFT REGISTER MECHANISM

The proposed concept of bicolor pulsed lasing in a shared cavity is schematically illustrated in Fig. 1, showcasing the transition from the initial pulse build-up to the stationary state.

The key role in bicolor pulsed lasing is played by the kilometer-long Raman fiber. This P_2O_5-fiber features a Raman gain spectrum with a quite narrow (~60 cm^{-1}) peak at a frequency shift of 1330 cm^{-1} [14,15]. This gain peak can provide efficient Raman conversion and amplification for relatively narrowband radiation, acting as an effective spectral filter. The P_2O_5-fiber has high normal chromatic dispersion in the operating spectral range of the proposed laser. However, it is important to emphasize that the proposed method does not involve any intracavity dispersion compensation or management. On the contrary, the dispersion-induced group velocity mismatch between the pump and Stokes waves in this fiber is one of the key factors for the bicolor pulse shaping and shift-register-like operation.

Amplification of the fundamental radiation at 1066 nm is provided through stimulated emission in a conventional, relatively short (4.5 m) Yb-doped fiber (which also has normal dispersion), pumped by CW radiation at 976 nm.

The development of the bicolor pulsed lasing from build-up to the stationary state can be described and explained phenomenologically as follows. First, as the pump power at 976 nm increases, the lasing threshold for CW generation at 1066 nm is approached. Subsequently, with the increased CW lasing power at 1066 nm, we approach the threshold of Raman lasing at 1241 nm. At this stage, inherent temporal fluctuations in CW lasing power at 1066 nm play a critical role in Raman pulse build-up. Due to the ultrafast nature of the Raman gain, above-threshold noisy spikes of the radiation at the fundamental wavelength lead to corresponding temporal variations of the Stokes wave. When traveling in the fiber with Raman amplification, initial temporal bursts of the Stokes radiation consume lumped portions of the pumping CW radiation, creating local temporal power drops. Owing to chromatic dispersion, the Raman bursts travel faster than the residual pump dips. Consequently, the leading edge of a Raman pulse always experiences stronger amplification than its trailing edge, which impacts the corresponding pumping wave spike. This mutual pulse cross-shaping at pump and Stokes waves is an important mechanism that facilitates the switch from the initial CW lasing at 1066 nm to dual-wavelength pulsed operation.

Steady-state pulse generation with dispersion-affected intracavity Raman conversion is possible when the superposition of pump and Raman pulses is reproduced after each round trip, at least in terms of the temporal distribution of the field intensities. This condition can be met for multi-pulse lasing when the laser cavity simultaneously hosts N equidistant pump pulses and $N-1$ equidistant Stokes pulses. As the cavity round trip time is inversely proportional to the speed of light in the medium and, thus, proportional to the frequency-dependent refractive index, $T_R = \frac{nL}{c}$, this leads to the following simultaneous requirements: $\frac{n_p L}{c} = N T_p$ and $\frac{n_S L}{c} = (N-1) T_S$, where T_p and T_S are periods in the pump and

Fig. 1. Schematics of the proposed concept of a shift register mechanism of pulsed operation. After initial bicolor pulse build-up and transition to steady state operation, the pump and Stokes pulse trains have the same pulse period T, equal to the differential group delay (DGD) introduced mostly by a kilometer-long high-dispersion Raman fiber. YDFA, ytterbium-doped fiber amplifier.

Stokes multi-pulse trains, respectively; n_p and n_S are the effective refractive indices of the P_2O_5-fiber (which constitutes the laser cavity) at the pump and Stokes wavelengths, respectively; L is the cavity length; c is the speed of light in vacuum.

The difference in the group velocities at two different wavelengths in the lengthy Raman fiber leads to the DGD $\Delta T_{DGD} = \frac{(n_p - n_S) L}{c}$, acquired during the intracavity round trip by the corresponding pulse trains at the pump and Stokes wavelengths. It is clear that the superposition of intensities of pump and Raman pulses can be reproduced after each round trip when $T_p = T_S = T = \Delta T_{DGD}$. Thus, the pulse repetition rate of the generated pump and Stokes pulses is

$$f_{rep} = \frac{1}{\Delta T_{DGD}} = \frac{c}{L \cdot (n_p - n_S)}. \qquad (1)$$

Thus, the DGD ΔT_{DGD} determines the achievable pulse repetition rate.

The critically important action of the proposed pulse shaping mechanism is the effective spectral filtering provided by the narrow width of the Raman gain peak at a frequency shift of 1330 cm^{-1} in the P_2O_5-fiber. The narrow gain stabilizes pulsed operation via the effective spectral filtering of the Stokes pulses, thereby preventing an excessive rise in their energy, similar to the well-known mechanism of dissipative soliton formation [22].

Note that in a general case, the laser cavity may contain other elements introducing extra DGD. Even in such a case, the pulse period will be primarily defined by the DGD accumulated in the Raman fiber, because the bicolor pulse shaping takes place predominantly in this part of the cavity. Introduction of extra DGD leads only to a small correction of the period by a value of the

order of $\delta T \cong \frac{\Delta T_{DGD}}{N}$. The above phenomenological description of the proposed laser operation concept is corroborated by the experiments and numerical modeling presented below.

3. EXPERIMENTAL RESULTS

A. Achieving Bi-chromatic Pulsed Operation

The experimental setup used to examine and validate the proposed mechanism of bicolor pulsed lasing is described in Supplement 1 Note S1. Briefly, a typical ring configuration of a Yb-based all-fiber laser (capable of CW lasing at 1066 nm) was used as a basis and then modified to incorporate a 1-km-long P_2O_5-fiber, which provided intracavity Raman amplification at a frequency shift of 1330 cm^{-1}. Bi-chromatic pulsed lasing was achieved by CW pumping of the Yb-doped active fiber at a wavelength of 976 nm using a high-power laser diode. This diode operated continuously in the constant-current mode. The fundamental and Stokes radiations were extracted after the corresponding intracavity amplification stages: after the Yb-doped fiber and after the Raman P_2O_5-doped fiber, respectively. Wavelength separation was additionally ensured using an external dichroic filter. The extracted fundamental and Stokes radiations were guided to the following measurement equipment: (i) a wavelength-calibrated digital power meter, (ii) a high-resolution (0.02 nm) spectrometer for characterizing their spectral properties, and (iii) two identical fast (5 GHz) photodiodes for time–frequency characterization of the fundamental and Stokes pulse trains using a real-time oscilloscope (16 GHz bandwidth) and a wideband RF spectrum analyzer.

The measured output power characteristics of the test-bed laser are shown in Fig. 2. This figure depicts the dependencies of the

laser's average output powers at 1066 nm (fundamental wavelength) and 1241 nm (Stokes wavelength) on the CW pump power at 976 nm. The data obtained from these measurements suggest that the emergence of the Stokes radiation can be traced back to surpassing the Raman lasing threshold when the lasing power at the fundamental wavelength reaches a sufficiently high level.

The bicolor pulsed regime is automatically triggered once the Raman lasing threshold is reliably surpassed with CW pump power at 976 nm reaching above 4.5 W. This pulsed operation can then be maintained at any arbitrarily high level of pump power available in the experiment. This observation is supported by consecutive oscilloscopic measurements as shown in Fig. 3, which were carried out at different pump power levels.

Figure 4 presents the evolution of the optical spectra of laser radiation around the fundamental (1066 nm) and Stokes (1241 nm) wavelengths as pump power at 976 nm is gradually increased. These measured optical spectra confirm the effective intracavity spectral filtering offered by the P_2O_5-fiber, which has a narrow Raman gain peak at a frequency shift of 1330 cm^{-1}. The spectral width of Raman radiation is noticeably narrower than that of fundamental radiation when compared at the same pump power.
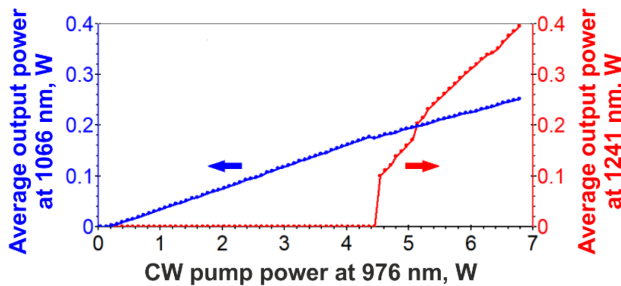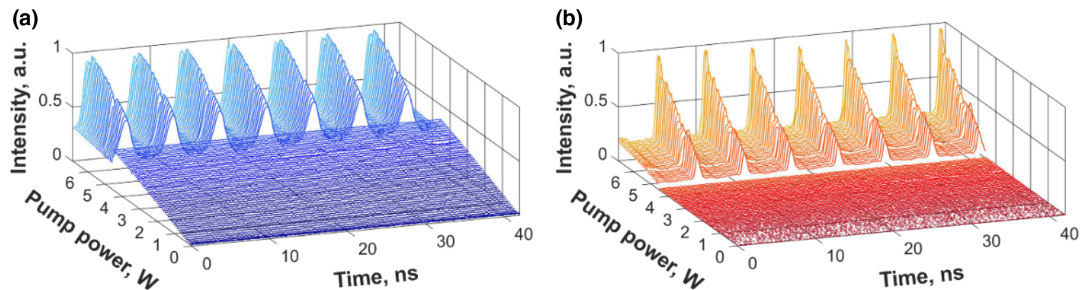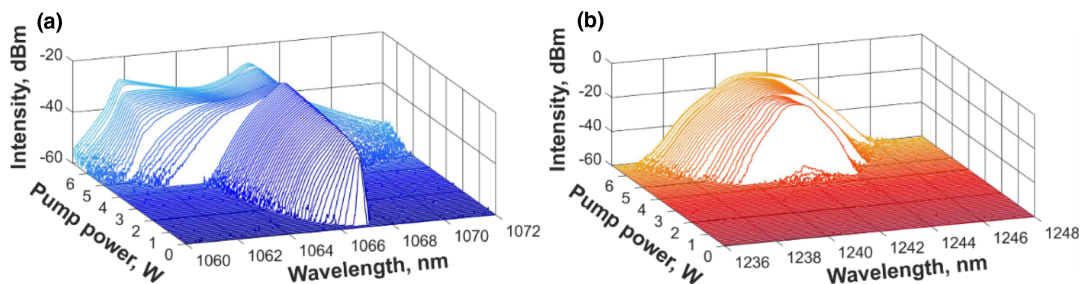
Throughout the power range limited by the highest available pump power, the laser exhibits remarkable stability with no significant change in the duration and period of the generated pulses. However, as the pump power nears the maximum available, the pulsed output becomes marginally noisier with decreased contrast. The following discussion will focus on the characteristics measured at a moderate pump power level of ∼5 W.
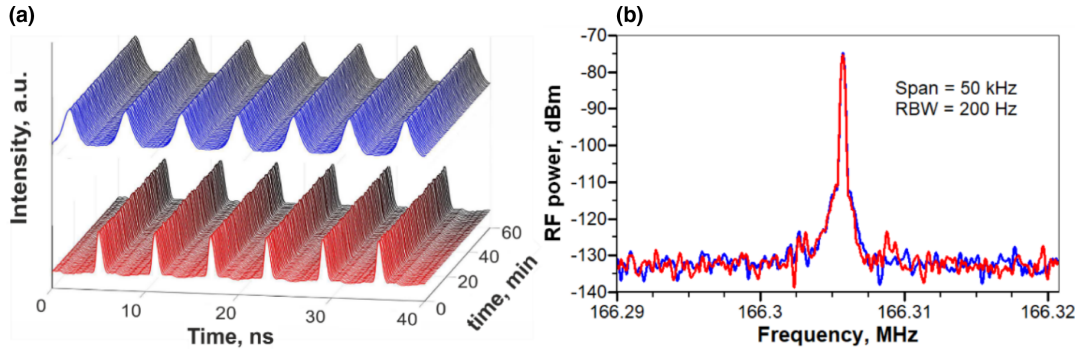
B. Validating the Regularity and Synchronization of Bi-chromatic Pulse Trains

By using an oscilloscope with a 16 GHz bandwidth, together with a suitably rapid photodiode, we measured the pulse duration of approximately 1.6 ns at 1066 nm, while at 1241 nm, it was around 0.7 ns. The pulse period was found to be about 6 ns for each pulse train, aligning well with the estimate made for the DGD in the Raman fiber.

The stability of pulse generation was evaluated by observing lengthy discrete series of time trace pairs, collected at 1 min intervals over the course of 1 h, as depicted in Fig. 5(a). These observations provided qualitative evidence of regular, synchronized, and stable pulse trains at both 1066 and 1241 nm.

We have also performed a quantitative evaluation of the noise characteristics and the synchronization of pulse repetition rates, by comparing the RF spectra of these pulse trains. The overlay of high-resolution RF spectra for the fundamental and Stokes pulse trains is displayed in Fig. 5(b). These spectra, recorded near the actual pulse repetition frequency of approximately 166.3 MHz, demonstrated a relatively high signal-to-noise ratio (≥ 50 dB). Moreover, they confirmed, via their frequency coincidence, that the pulse repetition rates at 1066 and 1241 nm wavelengths were indeed equal.

In addition to synchronization of pulse repetition rates, the measurement of the RF spectra also revealed remarkable suppression of supermode beat (SMB) noise (see Fig. 6).

Fig. 2. Measured output power characteristics of the laser: dependences of the average output powers at 1066 and 1241 nm on CW pump power at 976 nm.

Fig. 3. Time traces of laser radiation intensity at (a) 1066 nm and (b) 1241 nm acquired upon gradual increase of pump power at 976 nm from zero to the maximum.

Fig. 4. Optical spectra of laser radiation at (a) 1066 nm and (b) 1241 nm acquired upon gradual increase of pump power at 976 nm from zero to the maximum.

Fig. 5. (a) Series of time traces acquired during an hour (every minute) synchronously for the pulse trains at 1066 nm (upper traces) and 1241 nm (lower traces). (b) Overlay of the high-resolution RF spectra of 1066 and 1241 nm pulse trains measured in the vicinity of the actual pulse repetition frequency. RBW, resolution bandwidth.
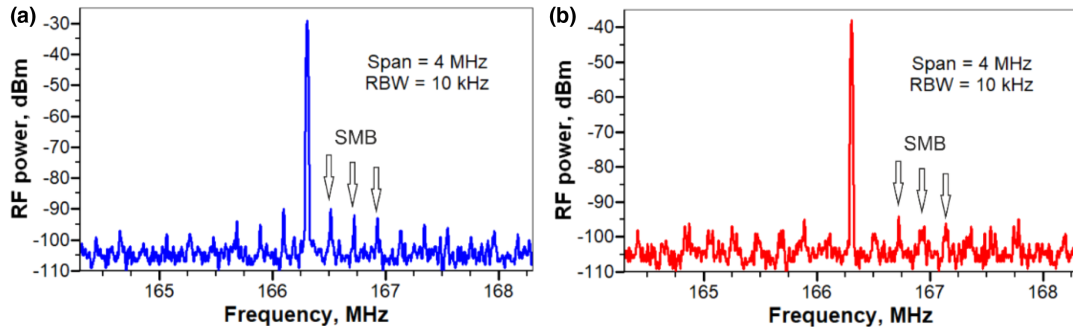
Fig. 6. Measured RF spectra of pulse trains generated at (a) 1066 nm and (b) 1241 nm, which manifest strong suppression of supermode beat (SMB) noise. RBW, resolution bandwidth.

SMBs are typically observed in the RF spectra of harmonically mode-locked lasers, i.e., lasers whose cavities host a number of uniformly distributed pulses. SMBs appear at frequencies that are multiples of the free spectral range (FSR) of the laser cavity [23]. This unwanted effect results from minor irregularities in a pulse train circulating within the laser cavity. Greater suppression of SMB noise corresponds to a higher degree of regularity in the pulse train. In the laser under study, the SMB noise suppression ratio exceeded 55 dB, as seen in Fig. 6. Consequently, the shift register operation mode is able to maintain a highly regular structure of the bi-chromatic pulse trains within the 1-km-long laser cavity, even with an extremely large number of pulses in those trains (exceeding 800 pulses at each wavelength, as estimated according to the actual pulse repetition rate of ~166.3 MHz and the cavity FSR of ~0.2 MHz).

4. THEORETICAL VALIDATION OF THE SHIFT REGISTER PULSE SHAPING MECHANISM

To validate the phenomenological description of the shift register pulse shaping presented in Section 2 and to gain a deeper understanding of this underlying physical mechanism, we utilized a numerical model of the bi-chromatic pulsed lasing regime. It is important to emphasize that we intentionally employed the simplest possible model, which incorporates only the essential physical effects not strictly specific to the fiber used in the experiment, to demonstrate the generality of the proposed approach and the feasibility of its implementation in different systems. This minimal model allows us to identify the primary underlying physical mechanisms responsible for pulse formation in the system under consideration. Specifically, our model is based on a well-established

system of two interconnected transport equations for the pump and Stokes waves. As the fundamental equation of wave dynamics, the transport equation has a general solution in the form of a wave with arbitrary shape that propagates at a specified velocity. To simulate the system under study, we incorporated lumped losses and lumped amplification for the fundamental wave, along with distributed Raman interaction of the two waves, into the main equations for the pump and Stokes waves:

$$\frac{1}{v_p}\frac{\partial}{\partial t}P_p + \frac{\partial P_p}{\partial z} + \frac{\omega_p}{\omega_S}g_S P_S P_p + \alpha_p^{(1)}P_p\delta(z) + \alpha_p^{(2)}P_p\delta(z-L)$$

$$- \frac{g_0 P_p \delta(z-L)}{1 + \frac{\bar{P}_p}{P_{\text{sat}}}} = 0, \tag{2}$$

$$\frac{1}{v_S}\frac{\partial P_S}{\partial t} + \frac{\partial P_S}{\partial z} - g_S P_p P_S + \alpha_S^{(1)}P_S\delta(z) + \alpha_S^{(2)}P_S\delta(z-L)$$

$$+ \alpha_S^{(\text{eff})}(P_S)\cdot P_S\delta(z-L) = 0, \tag{3}$$

where t stands for time, ω denotes a carrier frequency, and z is the longitudinal coordinate along the P_2O_5-doped fiber of length $L = 1$ km; P represents the intra-cavity power, and subscripts p and S denote pump and Stokes waves, respectively. Additionally, v is the group velocity; $g_S = 1.3$ W^{-1}km^{-1} is Raman gain; $\alpha^{(1)}$ and $\alpha^{(2)}$ stand for lumped losses introduced by the output couplers placed at the beginning ($z = 0$) and at the end ($z = L$) of the P_2O_5-doped fiber ($1.5 + 1.5$ dB for pump and $3.0 + 7.0$ dB for Stokes wave), respectively; δ stands for the Dirac delta function. To ensure that observed pulsed dynamics are not due to

self-induced oscillations of the Yb amplifier, we used the simplest model for saturated gain, as seen in the last term of Eq. (2). Here, g_0 stands for the small-signal gain coefficient; P_{sat} is the saturation power of the Yb amplifier; $\bar{P}_p$ is time-averaged pump power; pump amplification is assumed to be lumped, $g(z) \sim \delta(z - L)$, since the Yb optical amplifier length is much less than total cavity length. The last term of Eq. (3) accounts for effective power loss that simulates a decrease in the efficiency of Raman interaction between the two waves due to self-phase modulation, which leads to spectral broadening and thus results in power exiting outside of the Raman peak bandwidth. We utilized here a power loss law for the Gaussian spectrum $\alpha_S^{(eff)} = (1 + (\sigma_S P_S)^2)^{-\frac{1}{2}}$, provided that spectral width is proportional to power level. In what follows, we use $\sigma_S \sim 0.1 \text{ W}^{-1}$; however, varying σ_S approximately by an order of magnitude allowed us to reproduce qualitatively the same results. For further information on the model used for effective nonlinear spectral filtering, see Supplement 1 Note S2.

Given that the optical fiber forms a cavity, we applied periodic boundary conditions $P_{p,S}(L) = P_{p,S}(0)$ to Eqs. (2) and (3). For the initial conditions, we introduced weak noise with a randomly varying amplitude at the micro-Watt level. To numerically integrate Eqs. (2) and (3), we utilized a uniform mesh with $N = 10^5$ points and a step size h of approximately 1 cm. We verified that the results were consistent when using twice the number of mesh points. To integrate over time t, we employed a stable first-order numerical scheme with a time step $h n_S / c \sim 50 \text{ ps}$. To simulate the start-up of pulsed operation, we adiabatically increased P_{sat} from 10 µW up to approximately 200 mW over the first 200 cavity round trips, while keeping g_0 fixed at 15 dB. Subsequently, we simulated an additional 1000 round trips at a constant P_{sat} to ensure that the lasing regime reached a steady state. To accurately reproduce pulse shaping near the Raman threshold, a much more adiabatic power increase is necessary, typically requiring 1 to 3×10^5 cavity round trips. To complete the simulation in a reasonable time, we employed a cavity scaling factor $M \sim 5 \ldots 20$, which reduced the number of mesh points $N \rightarrow N/M$ and cavity length $L \rightarrow L/M$. At the same time, we increased the Raman gain by a factor of M: $g_s \rightarrow M g_s$, as well as group velocity difference $v_S - v_p$. This approach allowed us to accelerate the simulation by a factor of M^2. Specifically, Fig. 7 was generated using $M = 10$. Once the pump power is well above the Raman threshold, the results are virtually independent of the scaling factor M. For more information on the numerical modeling speed-up technique and its validation, see Supplement 1 Note S3.

Figure 7 shows a series of time traces of laser radiation intensity obtained with this model. It is important to note that these graphs bear a strong resemblance to the experimental ones depicted in
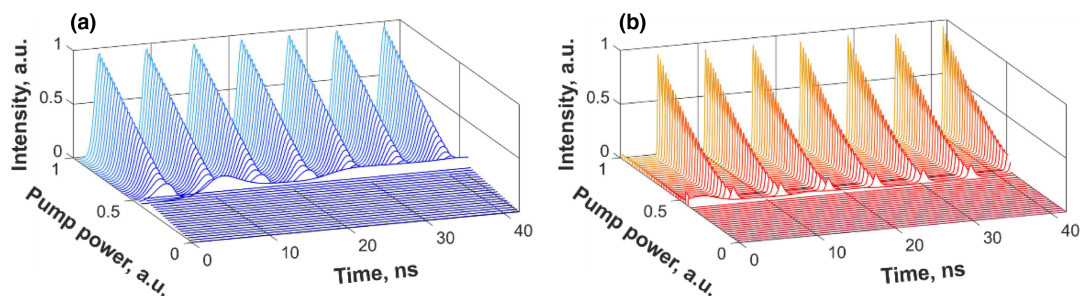
Fig. 3. Thus, the radiation power at a wavelength of 1066 nm increases almost linearly until reaching the threshold for Stokes wave generation, at which point pulsed generation occurs for both waves. The period of the pulse train generated is determined by DGD and is approximately 6 ns. A slight discrepancy from the experimental data is observed in the form of a narrow transition region with irregular pulsing near the Stokes wave generation threshold and slightly improved contrast of the generated pulses.

Overall, the results of the numerical simulation are in reasonably good agreement with the experimental observations, which confirms the accuracy of our understanding of the new mechanism of pulsed generation incorporated within our numerical model.

5. DISCUSSION

In this section, we discuss the generality of the proposed method. In particular, we consider the possibility of varying the output light characteristics and the feasibility of extending the technique to other active media and laser designs.

In accordance with the basic principle of the proposed shift register mechanism, the repetition period of the generated bicolor pulses is determined by their DGD in the Raman fiber, which, in turn, is determined by the length of this fiber [see Eq. (1)]. A significant change in the length of the Raman fiber (and overall cavity dispersion) should also affect the pulse duration. To validate the feasibility of such control over the temporal characteristics, we reduced the length of the P_2O_5-fiber from ∼1 to ∼0.65 km and performed experimental measurements and numerical simulations of pulsed lasing in such a shortened laser cavity. As expected, the pulse repetition frequency increased from 166.3 to 249.1 MHz. At the same time, the pulse duration decreased by approximately the same factor: the fundamental pulse duration reduced to ∼0.99 ns, while the Stokes pulse duration became ∼0.42 ns. The experimental and theoretical data confirming this are provided in Supplement 1 Note S4. Therefore, by varying the length of the Raman fiber, one can control the temporal characteristics of bicolor pulsed generation. We estimate that further reduction of the P_2O_5-fiber length (combined with an appropriate decrease in the output coupling ratio for the Stokes radiation to maintain the lasing threshold at an accessible pump power level) will make it possible to achieve a pulse duration of about 0.1 ns at a pulse repetition rate of about 1 GHz.

Another possible way to manipulate both temporal and spectral characteristics of the proposed lasing method is to exploit materials with a Raman frequency shift different from the one used in our P_2O_5-fiber-based laser configuration. We anticipate that the proposed method can be extended to different Raman fibers, including conventional glass fibers with the Raman frequency shift of 440 cm^{-1}. In that case, the absence of a such narrow peak in the

Fig. 7. Time traces of laser radiation intensity at (a) 1066 nm and (b) 1241 nm acquired from the theoretical model upon gradual increase of amplifier saturation power level P_{sat} from zero to the maximum.

Raman gain spectrum, as in the P_2O_5-fiber, can be compensated for by installing a real passband filter into the laser cavity. The numerical simulation (presented in the previous section) suggests that such a substitution is possible, since the effective nonlinear spectral filtering was considered as a lumped term in Eq. (3) used to model pulsed lasing at the Stokes wavelength. Thus, the lumped filtering is shown to be sufficient for stabilization of the shift register bicolor pulsed lasing, similarly to the distributed effective spectral filtering in the P_2O_5-fiber. The ability to vary the Raman frequency shift opens the prospect for implementation of versatile control over the lasing wavelengths and their difference. Additionally, the possibility to vary the DGD provides a way to manipulate the repetition rate and duration of generated bicolor pulses.

It is also apparent that the proposed method can be implemented in lasers with various designs (all-fiber or hybrid (bulk/fiber)) and different amplifying media for the fundamental lasing wavelength. A general requirement for potential laser designs is the presence of a Raman medium with sufficient length to overcome the lasing threshold at the Stokes wavelength, along with a passband spectral filter (either real or effective) centered at this wavelength.

6. CONCLUSION

We have proposed a novel concept for generating dual-wavelength pulse trains in a single-cavity fiber laser and have validated it both theoretically and experimentally. The experimental demonstration of this new mechanism was performed using a combined rare-earth and Raman fiber laser. In this system, the dual-wavelength pulsed generation mechanism is based on the self-induced modulation of intracavity Raman conversion, facilitated by a combination of strong chromatic dispersion and the relatively narrow spectral width of the peak of Raman amplification. Meeting these two conditions allows simultaneous shaping of sub-nanosecond pulse trains at highly separated different wavelengths (e.g., 1066 and 1241 nm), without any material saturable absorbers or modulators.

The proposed new approach also inherently ensures the mutual synchronization of pulse repetition rates at both lasing wavelengths, without the necessity for special technical measures or precise adjustments. The repetition rate is determined by the dispersion-induced DGD acquired by generated bicolor pulses at every intracavity round trip, making it inherently high (>100 MHz).

It is important to stress that although we have employed a specific implementation for experimental demonstration, the method itself is quite generic and can be applied in various configurations and different practical solutions for energy transfer between pump and Stokes waves. We anticipate that the proposed and demonstrated novel approach to bicolor high-repetition-rate pulsed lasing will find a wide range of applications and will advance technologies such as LIDAR, laser spectroscopy, and the development of efficient mid-infrared light sources.

Disclosures. The authors declare no conflicts of interest.

Data availability. Not all data underlying the results presented in this paper are publicly available at this time (as restricted by a supervisory authority) but may be obtained from the authors upon reasonable request. Readers may email the corresponding author for that purpose. Some underlying data are also reported in Supplement 1.

Supplemental document. See Supplement 1 for supporting content.

REFERENCES

1. Q. Hao, C. Wang, W. Liu, X. Liu, J. Liu, and H. Zhang, "Low-dimensional saturable absorbers for ultrafast photonics in solid-state bulk lasers: status and prospects," Nanophotonics **9**, 2603–2639 (2020).
2. S. M. Kobtsev, "Artificial saturable absorbers for ultrafast fibre lasers," Opt. Fiber Technol. **68**, 102764 (2022).
3. B. Querzola, "High accuracy distance measurement by two-wavelength pulsed laser sources," Appl. Opt. **18**, 3035–3047 (1979).
4. F. M. Danson, R. Gaulton, R. P. Armitage, M. Disney, O. Gunawan, P. Lewis, G. Pearson, and A. F. Ramirez, "Developing a dual-wavelength full-waveform terrestrial laser scanner to characterize forest canopy structure," Agric. Forest Meteorol. **198**–199, 7–14 (2014).
5. C. Manzoni, O. D. Mücke, G. Cirmi, S. Fang, J. Moses, S.-W. Huang, K.-H. Hong, G. Cerullo, and F. X. Kärtner, "Coherent pulse synthesis: towards sub-cycle optical waveforms," Laser Photon. Rev. **9**, 129–171 (2015).
6. P.-T. Dong and J.-X. Cheng, "Pump–probe microscopy: theory, instrumentation, and applications," Spectroscopy **32**, 24–36 (2017).
7. T. Gottschall, T. Meyer, M. Baumgartl, C. Jauregui, M. Schmitt, J. Popp, J. Limpert, and A. Tunnermann, "Fiber-based light sources for biomedical applications of coherent anti-Stokes Raman scattering microscopy," Laser Photon. Rev. **9**, 435–451 (2015).
8. Y. Sasaki, H. Yokoyama, and H. Ito, "Dual-wavelength optical-pulse source based on diode lasers for high-repetition-rate, narrow-bandwidth terahertz-wave generation," Opt. Express **12**, 3066–3071 (2004).
9. N. Zhao, M. Liu, H. Liu, X.-W. Zheng, Q.-Y. Ning, A.-P. Luo, Z.-C. Luo, and W.-C. Xu, "Dual-wavelength rectangular pulse Yb-doped fiber laser using a microfiber-based graphene saturable absorber," Opt. Express **22**, 10906–10913 (2014).
10. K. Y. Lau, M. H. Abu Bakar, F. D. Muhammad, A. A. Latif, M. F. Omar, Z. Yusoff, and M. A. Mahdi, "Dual-wavelength, mode-locked erbium-doped fiber laser employing a graphene/polymethyl-methachrylate saturable absorber," Opt. Express **26**, 12790–12800 (2018).
11. R. Liao, Y. Song, W. Liu, H. Shi, L. Chai, and M. Hu, "Dual-comb spectroscopy with a single free-running thulium-doped fiber laser," Opt. Express **26**, 11046–11054 (2018).
12. Y. Li, K. Zhao, B. Cao, X. Xiao, and C. Yang, "Carbon nanotube-synchronized dual-color fiber laser for coherent anti-Stokes Raman scattering microscopy," Opt. Lett. **45**, 3329–3332 (2020).
13. S. A. Hussain, "Ultrashort dual colour laser at 1.55 and 1.88 μm by using a carbon nanotube saturable absorber," IEEE Photon. Technol. Lett. **31**, 990–993 (2019).
14. V. G. Plotnichenko, V. O. Sokolov, V. V. Koltashev, and E. M. Dianov, "On the structure of phosphosilicate glasses," J. Non-Cryst. Solids **306**, 209–226 (2002).
15. G. Salceda-Delgado, A. Martinez-Rios, B. Ilan, and D. Monzon-Hernandez, "Raman response function and Raman fraction of phosphosilicate fibers," Opt. Quantum Electron. **44**, 657–671 (2012).
16. S. Kobtsev, S. Kukarin, and A. Kokhanovskiy, "Synchronously pumped picosecond all-fibre Raman laser based on phosphorus-doped silica fibre," Opt. Express **23**, 18548–18553 (2015).
17. D. S. Kharenko, V. D. Efremov, E. A. Evmenova, and S. A. Babin, "Generation of Raman dissipative solitons near 1.3 microns in a phosphosilicate-fiber cavity," Opt. Express **26**, 15084–15089 (2018).
18. S. Kobtsev, A. Ivanenko, A. Kokhanovskiy, and M. Gervaziev, "Raman-converted high-energy double-scale pulses at 1270 nm in P_2O_5-doped silica fiber," Opt. Express **26**, 29867–29872 (2018).

19. S. A. Babin, E. V. Podivilov, D. S. Kharenko, A. E. Bednyakova, M. P. Fedoruk, V. L. Kalashnikov, and A. Apolonski, "Multicolour nonlinearly bound chirped dissipative solitons," Nat. Commun. **5**, 4653 (2014).

20. D. S. Kharenko, A. E. Bednyakova, E. V. Podivilov, M. P. Fedoruk, A. Apolonski, and S. A. Babin, "Feedback-controlled Raman dissipative solitons in a fiber laser," Opt. Express **23**, 1857–1862 (2015).

21. S. Chang, H. Wang, Z. Wang, and H. Yang, "Generation of coherent multicolor noise-like pulse complex in Yb-doped fiber laser mode-locked by GIMF-SA," Opt. Express **29**, 14336–14344 (2021).

22. F. W. Wise, A. Chong, and W. H. Renninger, "High-energy femtosecond fiber lasers based on pulse propagation at normal dispersion," Laser Photon. Rev. **2**, 58–73 (2008).

23. O. Pottiez, O. Deparis, R. Kiyan, M. Haelterman, P. Emplit, P. Megret, and M. Blondel, "Supermode noise of harmonically mode-locked erbium fiber lasers with composite cavity," IEEE J. Quantum Electron. **38**, 252–259 (2002).